Zonal jets in the Southern Ocean: a semi-analytical model based on scale separation

S. Elnaz Naghibi*[a], Sergey A. Karabasov[b], Igor Kamenkovich[c]

[a] Department of Aeronautics, Imperial College London

[b] School of Engineering and Materials Science, Queen Mary, University of London

[c] Rosenstiel School of Marine, Atmospheric and Earth Science, University of Miami

Abstract

A reduced-order semi-analytic model of multiple zonal jets in the Southern Ocean is proposed based on the statistical approach and scale decomposition. By introducing two dominant scales in the vorticity equation, the model describes the large-scale and mesoscale dynamics using the explicit momentum dissipation in the horizontal and vertical directions. For validation and physical insights, the results of the reduced-order model are compared with solutions of two eddy-resolving ocean models: i) a realistic primitive-equation HYCOM (HYbrid Coordinate Ocean Model) simulation of the Southern Ocean and ii) an idealized quasi-geostrophic model of a shear-driven channel flow.

1. Introduction

Multiple zonal jets, oriented in the east-west direction while alternating in the latitudinal direction, are observed in different regions of the global oceans as reported from velocity observations and satellite altimetry data [1-4]. The emergence of zonal jets is similarly confirmed by numerical ocean models run in eddy-resolving regimes [5-9]. A similar persistent pattern of zonal jets is also observed in atmospheres of giant planets such as Jupiter and Saturn [10, 11]. In addition to visual resemblance, the analysis on energy spectra in these cases indicates the same underlying dynamics [12]. Development of physically insightful mathematical models of the structure and dynamics of zonal jets remains one of the active research directions in planetary sciences.

Among other techniques, linear stability and nonlinear perturbation methods are popular tools to analyze the dynamics of zonal jets in the literature. For example, Kaspi and Flierl (2007) considered baroclinic instability and nonlinear interactions between eddies as the formation mechanism of jets in the atmosphere of gaseous planets using a nonlinear analytical model [13]. Farrel and Ioannou (2008) used the stochastic structural stability theory to study the interaction of

jets with turbulence for a two-layer baroclinic model and explain the physical mechanism behind the formation and maintenance of baroclinic jets [14]. Along a similar line of thought, Berloff et al. (2009) considered a two-stage development process of the formation of zonal jets [15]. First, the energy of the background flow is released to long meridional and short zonal length scales via a linear mechanism. Then a secondary instability occurs, which sets the meridional scale of the zonal jets [15]. Furthermore, Connaughton et al. (2010) studied modulational instability of geophysical Rossby and plasma drift waves as a formation mechanism of zonal jets both theoretically and numerically using Charney–Hasegawa–Mima model [16].

At the other end of the spectrum, there are statistical models of zonal jets such as those considering the inverse energy cascade in beta plane turbulence. The focus of these models tends to be in the zonal jet structure and their maintenance mechanism at an advanced stage once the jets reach the state of statistical stationarity. The key concept here pioneered by Rhines (1994) [17] is the so-called halting length scale, which emerges from the analysis of the wavenumber spectrum for turbulence energy. This scale divides the beta plane turbulence into isotropic small scales and highly anisotropic large scales that form the zonal jets. The Rhines scale depends on r.m.s. velocity and the gradient of the Coriolis parameter. In a further study [18], the Rhines scale together with a second length-scale, which describes the forcing strength with respect to the background potential vorticity gradient, were reported to determine the structure of zonal jets. In the work by Danilov and Gurarie [19], Rhines' theory was further extended to account for bottom friction effects. In addition, Nadiga (2006) related the development of zonal jets to a detention of the turbulent inverse-cascade of energy by free Rossby waves, which are subsequently redirected into zonal modes [20].

A different approach was considered by Huang and Robinson (1998) [21] who showed that the persistent jets are mainly maintained by the shear-straining between small-scale eddies and large-scale zonal jets. This work demonstrated an evident scale separation between the small eddy scale and the large jet scale. It was also shown that despite a similarity between the Rhines scale and the jet scale, they are not obviously linked statistically [21].

The current work exploits the separation between the long scale of the background flow and the short jet scale to develop a close-form semi-analytical model, which is amenable to fast turn-around solution ideally suitable for parametric studies. The goal of the model is to explicitly

capture interaction between spatial scales in a realistic flow regime with strong vertical shear and mixing and non-negligible vertical velocities. The balance at each scale is preserved due to viscosity, thereby explicitly illustrating the importance of momentum dissipation. The balance serves as an equilibration mechanism for turbulence generated by large-scale forcing, which maintains zonal jets in a statistically stationary regime. Section 2 shows how the assumed scale separation allows to reduce the governing equations into two separate sets of equations, one for the large-scale background flow and the other for the small-scale zonal jets, each of which is solved semi-analytically. It is shown that the wind-stress forcing and the bottom friction dissipation mainly govern the large-scale vorticity dynamics, which can be solved separately from the zonal jets equation. The parameters of the semi-analytical statistical model are derived from the time- and zonally- averaged dynamics of the Southern Ocean as simulated by general circulation HYCOM model. In Section 3, the developed model is first validated in comparison with the HYCOM solution. To examine how robustly the semi-analytical model captures the fundamental underlying physics, the same calibration process is then further applied to the quasi-geostrophic solution of the zonal channel.

2. Methodology

2.1 Primitive equation model

The governing equations for ocean dynamics in z-level coordinates can be described by the conservation laws for momentum, temperature, salinity and mass, as well as the equation of state:

$$
\begin{aligned}
&\frac{\partial \mathbf{v}}{\partial t} + \left(\mathbf{v}.\nabla\right)\mathbf{v} + 2\boldsymbol{\omega}\times\mathbf{v} = \mathbf{g} - \frac{\nabla P}{\rho} + \frac{\nabla.\boldsymbol{\tau}}{\rho},\\
&\frac{\partial T}{\partial t} + \nabla.\left(T\mathbf{v}\right) = \nabla.\left(\kappa\nabla T\right) + F^{T},\\
&\frac{\partial S}{\partial t} + \nabla.\left(S\mathbf{v}\right) = \nabla.\left(\kappa\nabla S\right) + F^{S},\\
&\nabla.\mathbf{v} = 0,\\
&\rho = \rho\left(T,S,P\right),
\end{aligned}
\qquad (1)
$$

where $\mathbf{v}$ is the velocity vector, $\boldsymbol{\omega} = \left(0,0,\Omega\right)$ is the Earth's angular velocity, P is pressure, $\mathbf{g}$ is the gravitational acceleration and $\boldsymbol{\tau}$ is a stress tensor (which includes viscosity). T and S are

temperature and salinity with F^T and F^S being the corresponding source terms in their conservation equations, κ is diffusivity tensor and ρ is the density.

In this study, we use solutions from a general ocean circulation HYCOM (HYbrid Coordinate Ocean Model). The model simulation results were downloaded from the HYCOM data portal (hycom.org), where they had been interpolated to z-level coordinates. The hybrid coordinates in the original simulation are isopycnal in the open, stratified ocean and smoothly transition to terrain-following sigma-coordinates in shallow coastal regions and to z-level coordinates in the mixed layer and unstratified seas [22]. The advection of heat and salt was computed using the improved advection scheme MPDATA [23, 24]. Following Brydon et al. [25], an approximation of the UNESCO equation of state was used. The Mellor-Yamada Level 2.5 turbulence closure algorithm was utilized to account for mixing from surface to bottom [26, 27]. The horizontal grid resolution was 1/12 degree in the longitude and latitude, and there were 41 vertical layers used.

Of particular interest in this work is the HYCOM solution in a sector of the Southern Ocean between latitudes of 37^0 S to 60^0 S ($\theta_1 = 2.2162$ and $\theta_2 = 2.6182$ radians in spherical coordinates (r, θ, ϕ) used in the reduced-order model) and in the longitudes, approximately between Montagu Island to Tasmania (20^0 W to 140^0 E i.e. $\phi_1 = -0.3491$ and $\phi_2 = 2.4435$ radians). This sector is carefully selected to avoid the continental boundaries, the effect of which would be difficult to include in low fidelity models.

Typical velocity solutions of HYCOM extracted over one-year period (January- December 2014) using five-day snapshots are shown in Fig.1. According to our analysis of HYCOM solution in a 5-year period (January 2013-Decemvber 2018), main spatial characteristics of zonal jets, which are the focus of this study, do not change with longer averaging period. It can be noted that the HYCOM-simulated currents in the selected region of interest are nearly zonal and can be approximated by a zonally-re-entrant flow in a channel, which is discussed next.

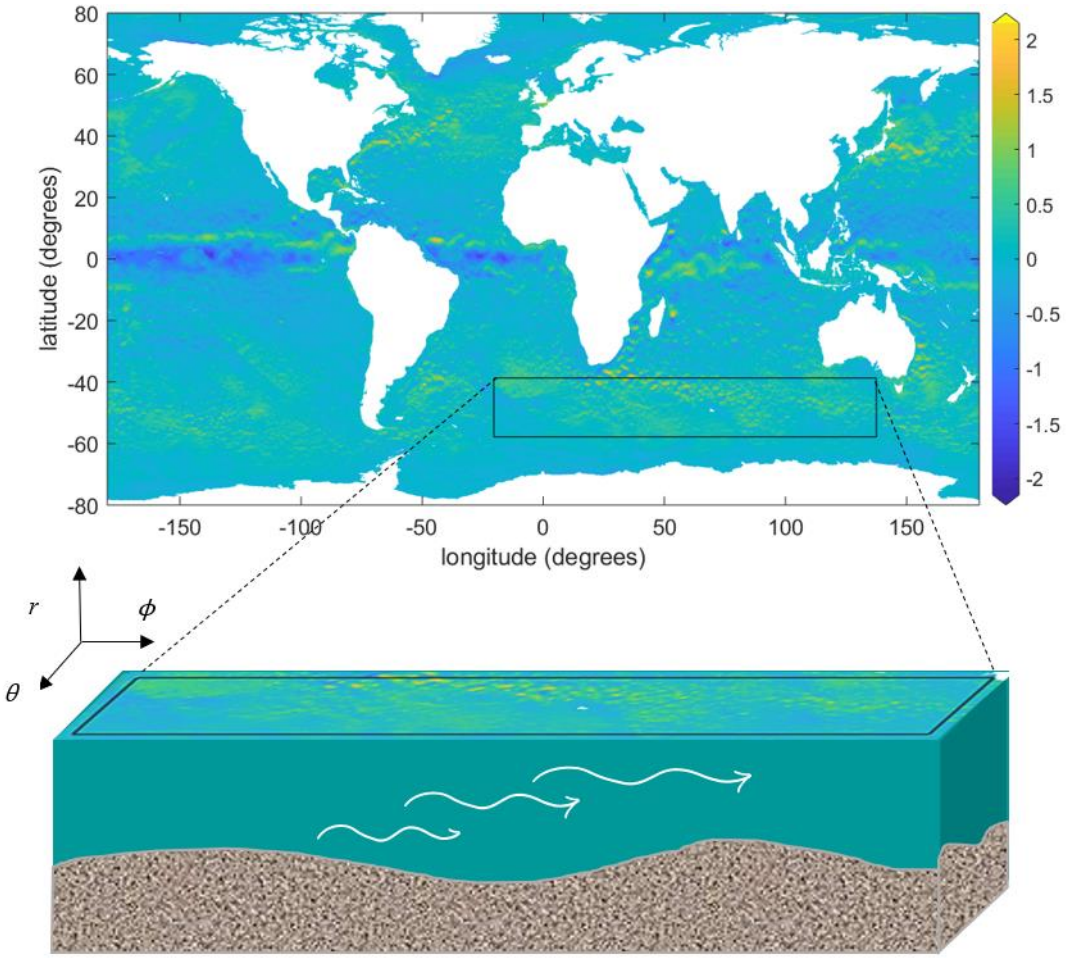

Fig. 1 Top panel: instantaneous distribution of the top-layer zonal velocity (ms^{-1}) in HYCOM, where the Southern Ocean region under study is shown in a box. Bottom panel: a schematic of the solution domain and the spherical coordinate system.

2.2 Quasi-geostrophic model

A quasi-geostrophic model was configured for a flow in a mid-latitude zonally re-entrant channel, with solid southern and northern walls and periodic conditions at west and east. The size of the computational domain corresponded to 3000km×12000km in latitudinal and longitudinal directions, respectively. The governing equations were the conservation of potential vorticity (PV) in the Cartesian coordinates for each of the three isopycnal layers considered. Dissipation was modeled by lateral viscosity and bottom friction in accordance with:

$$\partial_t q_i + J(\psi_i, q_i) = \nu \Delta^2 \psi_i - \delta_{i3} \gamma \Delta \psi_i, \; i = 1,2,3, \tag{2}$$

where $\gamma = 4.6 \times 10^{-8}$ m^{2}s^{-1} and $\nu = 10$ m^{2}s^{-1} are bottom friction and lateral viscosity coefficients, respectively. δ_{ij} is the Kronecker symbol, ψ_i is quasi-geostrophic stream function, q_i is the quasi-geostrophic potential vorticity, and $J(f,g) = f_x g_y - f_y g_x$. The three horizontal isopycnal layers were dynamically coupled through interface displacements. The flow was decomposed into the large-scale uniform background flow U_i and perturbations [7, 8, 9], so that

$$q_i = \nabla^2 \psi_i + \beta y - (1-\delta_{i1}) S_{i1} \left[\psi_i - \psi_{i-1} + (U_i - U_{i-1}) y \right] - (1-\delta_{i3}) S_{i2} \left[\psi_i - \psi_{i+1} + (U_i - U_{i+1}) y \right], i = 1,2,3, \tag{3}$$

where $\beta = 1.3 \times 10^{-11}$ m^{-1}s^{-1} is the Coriolis parameter gradient and the stratification parameters S_{i1} and S_{i2} were selected so that the first and second Rossby deformation radii would be $Rd_1 = 20$ km and $Rd_2 = 12$ km, respectively. The depths of the layers were $H_1 = 300$, $H_2 = 1100$ and $H_3 = 2600$ m numbered from the top and background velocities were $U_1 = 6, U_2 = 3, U_3 = 0$ cms^{-1}, respectively. On the zonal walls, no-slip boundary conditions were applied. The equations were numerically solved using the high-resolution CABARET scheme on a uniform Cartesian grid of 512×2048 cells [28, 29].

The results were obtained for a 10-year simulation after 4000 days of spinout time and stored every 10 days for the subsequent analysis. For illustration, the computed instantaneous vorticity distribution in the top layer is shown in Fig. 2.

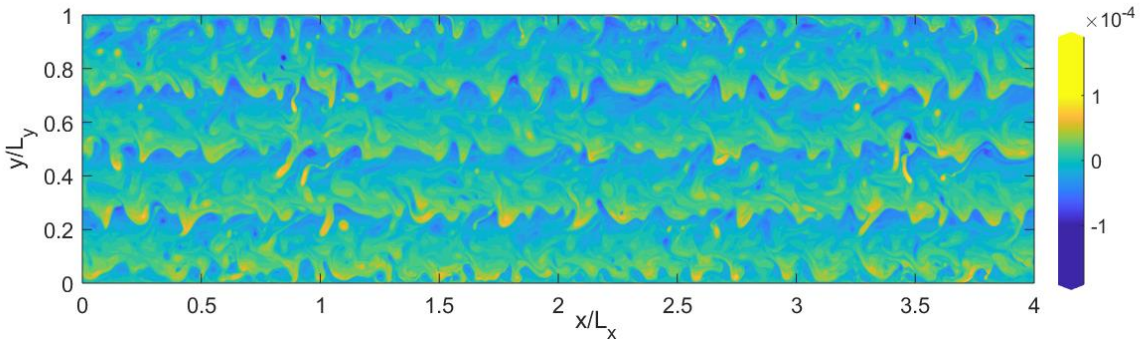

Fig. 2 Quasi-geostrophic model of the shear-driven zonal channel: instantaneous distribution of potential vorticity (s^{-1}) in the top layer.

2.3 Reduced-order model

2.3.1 Governing equations and assumptions

In this section, the reduced order model is derived from primitive equations, by first averaging the vorticity equation in time and in the zonal direction. The derivation process is then completed by formulating a closure model for the eddy viscosity and replacing the top and bottom boundary conditions with the equivalent body forces.

Following Pedlosky [30], let us take the curl of the momentum equation in Eq. (1). This leads to elimination of pressure gradients and conservative body forces and results in the equation for the relative vorticity vector, $\boldsymbol{\zeta}$,

$$\frac{\partial \boldsymbol{\zeta}}{\partial t} + (\mathbf{v}.\nabla)\boldsymbol{\zeta} + 2(\mathbf{v}.\nabla)\boldsymbol{\omega} = \nabla \times \left(\frac{\nabla.\boldsymbol{\tau}}{\rho} \right) + (\boldsymbol{\zeta}.\nabla)\mathbf{v} + 2(\boldsymbol{\omega}.\nabla)\mathbf{v}. \tag{4}$$

Here, spherical coordinates, (r,θ,ϕ) are used where r is the radial distance from the Earth's center, and θ and ϕ are respectively co-latitudinal (north to south) and azimuthal (west to east) angles as shown in Fig. 1. The velocity vector components in spherical coordinates are $\mathbf{v} = (v_r, v_\theta, v_\phi)$.

The continuity equation is given by

$$\frac{1}{r^2}\frac{\partial (r^2 v_r)}{\partial r} + \frac{1}{r\sin\theta}\frac{\partial (\sin\theta v_\theta)}{\partial \theta} + \frac{1}{r\sin\theta}\frac{\partial v_\phi}{\partial \phi} = 0. \tag{5}$$

The radial component of Eq. 4 describes the evolution of the vertical vorticity component, $\zeta = \frac{1}{r\sin\theta}\left(\frac{\partial}{\partial\theta}(\sin\theta v_\phi) - \frac{\partial v_\theta}{\partial \phi} \right)$:

$$\frac{\partial \zeta}{\partial t} = \frac{2\Omega}{r}\left[\sin\theta v_\theta + \frac{\cos\theta}{r}\frac{\partial (r^2 v_r)}{\partial r} \right] + I^{\text{conv}}(v_\theta, v_\phi) + \frac{a_h{}^L}{r^2\sin\theta}\frac{\partial}{\partial\theta}\left(\sin\theta \frac{\partial \zeta}{\partial\theta} \right) + \frac{a_h{}^L}{r^2\sin^2\theta}\frac{\partial^2 \zeta}{\partial \phi^2} + \frac{a_v}{r^3}\frac{\partial}{\partial r}\left[r^2 \frac{\partial}{\partial r}(r\zeta) \right], \tag{6}$$

where the nonlinear term is

$$I^{\mathrm{conv}}\left(v_\theta, v_\phi\right) = \frac{1}{r^2 \sin\theta}\left(\frac{\partial v_\theta}{\partial \phi}\frac{\partial v_\theta}{\partial \theta} + v_\theta \frac{\partial^2 v_\theta}{\partial \theta \partial \phi} + \frac{1}{\sin\theta}\frac{\partial v_\phi}{\partial \phi}\frac{\partial v_\theta}{\partial \phi} + \frac{v_\phi}{\sin\theta}\frac{\partial^2 v_\theta}{\partial \phi^2} - \sin\theta \frac{\partial v_\theta}{\partial \theta}\frac{\partial v_\phi}{\partial \theta} \right.$$

$$\left. -\sin\theta v_\theta \frac{\partial^2 v_\phi}{\partial \theta^2} - \cos\theta v_\phi \frac{\partial v_\theta}{\partial \theta} + \sin\theta v_\phi v_\theta - 2\cos\theta v_\theta \frac{\partial v_\phi}{\partial \theta} - \frac{\partial v_\phi}{\partial \theta}\frac{\partial v_\phi}{\partial \phi} - v_\phi \frac{\partial^2 v_\phi}{\partial \theta \partial \phi} - 2 v_\phi \cot\theta \frac{\partial v_\phi}{\partial \phi} \right). \quad (7)$$

In Eq. 6, $a_h{}^L$ and a_v are horizontal and vertical viscosity coefficients which represent the effect of small-scale mixing processes, not explicitly resolved by the model.

Next, Eq. 6 is integrated in time and in the zonal direction:

$$\iint \left\{ \frac{2\Omega}{r}\left[\sin\theta v_\theta + \frac{\cos\theta}{r}\frac{\partial\left(r^2 v_r\right)}{\partial r} \right] + I^{\mathrm{conv}}\left(v_\theta, v_\phi\right) + \frac{a_h{}^L}{r^2 \sin\theta}\frac{\partial}{\partial\theta}\left(\sin\theta \frac{\partial\zeta}{\partial\theta}\right) + \frac{a_h{}^L}{r^2 \sin^2\theta}\frac{\partial^2\zeta}{\partial\phi^2} + \frac{a_v}{r^3}\frac{\partial}{\partial r}\left[r^2 \frac{\partial}{\partial r}\left(r\zeta\right)\right] - \frac{\partial\zeta}{\partial t} \right\} \mathrm{r}\sin\theta\, \mathrm{d}\phi\, \mathrm{d}t = 0. \quad (8)$$

We then decompose the vorticity and all velocity components into the time- and zonal-mean and fluctuation parts denoted by the overbar and primes, respectively:

$$\zeta\left(r,\theta,\phi,t\right) = \overline{\zeta}\left(r,\theta\right) + \zeta'\left(r,\theta,\phi,t\right), v_\theta\left(r,\theta,\phi,t\right) = \overline{v_\theta}\left(r,\theta\right) + v_\theta{}'\left(r,\theta,\phi,t\right), v_\phi\left(r,\theta,\phi,t\right) = \overline{v_\phi}\left(r,\theta\right) + v_\phi{}'\left(r,\theta,\phi,t\right). \quad (9)$$

By definition, the mean fields satisfy

$$\frac{\partial\overline{\zeta}}{\partial t} = \frac{\partial\overline{v_\phi}}{\partial t} = \frac{\partial\overline{v_\theta}}{\partial t} = 0,$$
$$\frac{\partial\overline{\zeta}}{\partial \phi} = \frac{\partial\overline{v_\phi}}{\partial \phi} = \frac{\partial\overline{v_\theta}}{\partial \phi} = 0, \quad (10)$$

and the zonally averaged vorticity is expressed in terms of zonal velocity only

$$\overline{\zeta} = \frac{1}{r\sin\theta}\left(\frac{\partial}{\partial\theta}\left(\sin\theta \overline{v_\phi}\right)\right). \quad (11)$$

The difference between the time- and zonally averaged nonlinear term

$$\overline{I^{\mathrm{conv}}\left(v_\theta, v_\phi\right)} = \frac{1}{r^2 \sin\theta}\left(\overline{\frac{\partial v_\theta}{\partial \phi}\frac{\partial v_\theta}{\partial \theta}} + v_\theta \overline{\frac{\partial^2 v_\theta}{\partial \theta \partial \phi}} + \frac{1}{\sin\theta}\overline{\frac{\partial v_\phi}{\partial \phi}\frac{\partial v_\theta}{\partial \phi}} + \frac{1}{\sin\theta} v_\phi \overline{\frac{\partial^2 v_\theta}{\partial \phi^2}} - \sin\theta \overline{\frac{\partial v_\theta}{\partial \theta}\frac{\partial v_\phi}{\partial \theta}} \right.$$

$$\left. -\sin\theta v_\theta \overline{\frac{\partial^2 v_\phi}{\partial \theta^2}} - \cos\theta v_\phi \overline{\frac{\partial v_\theta}{\partial \theta}} + \sin\theta \overline{v_\phi v_\theta} - 2\cos\theta v_\theta \overline{\frac{\partial v_\phi}{\partial \theta}} - \overline{\frac{\partial v_\phi}{\partial \theta}\frac{\partial v_\phi}{\partial \phi}} - v_\phi \overline{\frac{\partial^2 v_\phi}{\partial \theta \partial \phi}} - 2\cot\theta v_\phi \overline{\frac{\partial v_\phi}{\partial \phi}} \right), \quad (12)$$

and the nonlinear term calculated from time- and zonally averaged velocities $I^{\mathrm{conv}}\left(\overline{v_\theta},\overline{v_\phi}\right)$ represents a contribution of the fluctuations ("eddies") to the mean vorticity balance and is approximated using the turbulence eddy viscosity

$$a_h{}^T\left[\frac{1}{r^2\sin\theta}\frac{\partial}{\partial\theta}\left(\sin\theta\frac{\partial\overline{\zeta}}{\partial\theta}\right)\right]=\overline{I^{\mathrm{conv}}\left(v_\theta,v_\phi\right)}-I^{\mathrm{conv}}\left(\overline{v_\theta},\overline{v_\phi}\right), \tag{13}$$

where $a_h{}^T$ is the turbulent eddy viscosity coefficient, which characterizes the effects of fluctuations ("eddies") on the large-scale flow as observed in high-Reynolds eddy-resolving simulations [9]. This coefficient is approximated using the classical Smagorinsky model [31],

$$a_h{}^T=\left(C_s\Delta\right)^2\left|\overline{S}\right|=\left(C_s\Delta\right)^2\sqrt{2\overline{S}_{ij}\overline{S}_{ij}}. \tag{14}$$

In the above, C_s is the standard dimensionless calibration parameter of the Smagorinsky model, S_{ij} is the rate of deformation tensor, which is an explicit function of velocity gradients, and $\overline{S}_{ij}$ is its time- and zonally-averaged value. The dynamic length scale Δ is used as the cut-off scale of the Smagorinsky model, which corresponds to the smallest scale explicitly resolved. The cut-off scale has been specifically adjusted for the considered ocean model. For example, if the velocity spectrum is dominated by a single meridional wavenumber K_θ i.e. $v_\phi\approx A_{\mathrm{k}_\theta}e^{iK_\theta R\left(\theta-\theta_1\right)}$, the largest dominant length scale is equal to the corresponding wavelength λ_θ, which sets up the cut-off scale equal to $\lambda_\theta/2$ [32],

$$\Delta=\frac{\lambda_\theta}{2}=\frac{\pi}{K_\theta}=\left|\pi v_\phi/\left(\frac{1}{R}\frac{\partial v_\phi}{\partial\theta}\right)\right|, \tag{15}$$

where $R=6371\,\mathrm{km}$ is the Earth's mean radius. Additionally, because the meridional geostrophic velocity is zero when averaged zonally above the topography and is generally much smaller than the zonal velocity in a channel configuration (Fig. 3), the former can be subsequently neglected. Given this and Eqs. 10, the nonlinear convection term $I^{\mathrm{conv}}\left(\overline{v_\theta},\overline{v_\phi}\right)$ is approximately zero. Hence, using the eddy viscosity model of Eq. 14, the mean vorticity equation (Eq. 8) reduces to

$$\frac{2\Omega}{r}\left[\sin\theta v_\theta + \frac{\cos\theta}{r}\frac{\partial\left(r^2 v_r\right)}{\partial r}\right] + \frac{a_h{}^L + a_h{}^T}{r^2\sin\theta}\frac{\partial}{\partial\theta}\left(\sin\theta\frac{\partial\zeta}{\partial\theta}\right) + \frac{a_v}{r^3}\frac{\partial}{\partial r}\left[r^2\frac{\partial}{\partial r}(r\zeta)\right] = 0, \tag{16}$$

or in an expanded form,

$$\frac{2\Omega}{r}\left[\sin\theta v_\theta + \frac{\cos\theta}{r}\frac{\partial\left(r^2 v_r\right)}{\partial r}\right] + \frac{a_h}{r^2}\left(\frac{\partial^2\zeta}{\partial\theta^2} + \cot\theta\frac{\partial\zeta}{\partial\theta}\right) + a_v\left(\frac{\partial^2\zeta}{\partial r^2} + \frac{4}{r}\frac{\partial\zeta}{\partial r} + \frac{2\zeta}{r^2}\right) = 0, \tag{17}$$

where bars are dropped for simplicity in presentation and $a_h = a_h{}^L + a_h{}^T$.

Since the ocean depth is much smaller than the average radius of the Earth ($\frac{H_{\max}}{R} << 1$), Eq. (17) is simplified by neglecting the terms $\frac{4}{r}\frac{\partial\zeta}{\partial r}$ and $\frac{2\zeta}{r^2}$

$$\frac{2\Omega}{r}\left[\sin\theta v_\theta + \frac{\cos\theta}{r}\frac{\partial\left(r^2 v_r\right)}{\partial r}\right] + \frac{a_h}{r^2}\left(\frac{\partial^2\zeta}{\partial\theta^2} + \cot\theta\frac{\partial\zeta}{\partial\theta}\right) + a_v\frac{\partial^2\zeta}{\partial r^2} = 0. \tag{18}$$

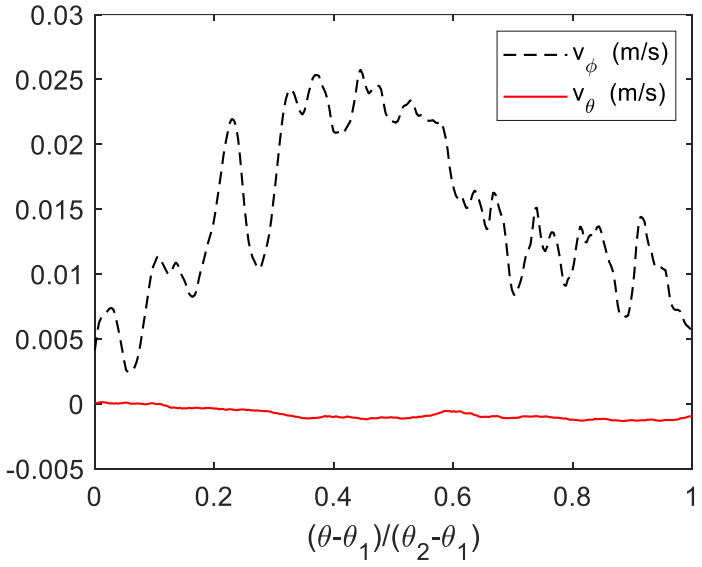

Fig. 3. Time, layer and zonally averaged profiles of the zonal and meridional velocity components in the HYCOM solution.

By filtering out zonal and temporal fluctuations, Eq. 18 describes the spatial structure of zonal- and time-mean relative vorticity subject to wind forcing and bottom friction. The Cartesian equivalent of Eq. 18 on a beta plane is derived in Appendix A highlighting the key differences of our model with the classical quasi-geostrophic equations.

The above equation needs to be simplified further to make it amenable to fast-turn-around-time and physically insightful semi-analytical solution methods. As the first step, the top and bottom boundary conditions are incorporated thereby simplifying the original boundary value problem. The velocity strain term is approximated by the wind stress assuming that in the top oceanic surface the momentum stress is determined by the zonal wind stress τ_ϕ :

$$a_v \frac{\partial v_\phi}{\partial r}|_{r=R} = \tau_\phi, \tag{19}$$

which corresponds to the surface sink/source of vorticity as follows:

$$a_v \frac{\partial \zeta}{\partial r}|_{r=R} = \frac{1}{r}\left[\frac{1}{\sin\theta}\left(\frac{\partial}{\partial\theta}\left(\sin\theta\tau_\phi\right)\right)\right]. \tag{20}$$

In the above equation a_v is taken to be $5\times10^{-3}\ \mathrm{m^2 s^{-1}}$ following the vertical diffusivity nominal value in HYCOM description [22] and $\tau_\phi = -\tau_{\phi_{\max}} \cos 2\pi \frac{\theta-\theta_1}{\theta_2-\theta_1}$ with $\tau_{\phi_{\max}} = 1\times10^{-4}\ \mathrm{m^2 s^{-2}}$ derived from the NAVGEM (Navy Global Environmental Model) 0.5-degree simulations. Fig. 4 confirms that the balance is well preserved for the HYCOM solution for the period January- December 2014.

Notably, the transfer of momentum from the wind acting on the surface to the ocean depth is governed by Ekman boundary layer. However, following [33] and similar low-resolution ocean models, the surface forcing is represented here by a body force Q^τ distributed over a depth of H_w in the upper ocean

$$Q^\tau = \frac{f(r)}{rH_w}\left[\frac{1}{\sin\theta}\left(\frac{\partial}{\partial\theta}\left(\sin\theta\tau_\phi\right)\right)\right],\ r_w < r < R, \tag{21}$$

where the top vertical profile function $f(r) = \mathrm{H}(r_w) - \mathrm{H}(R)$ is equal to unity in the interval $r_w < r < R$, with $r_w = R - H_w$ and $H_w = 7.5\ \mathrm{m}$, and H denotes the Heaviside step function.

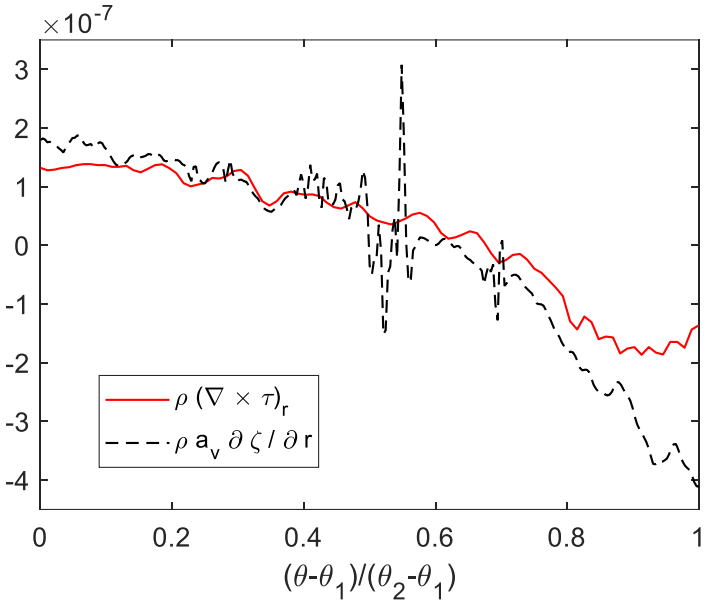

Fig. 4 Latitude profiles of the wind stress curl (NAVGEM 0.5 degree) and the vertical gradient of vorticity in the top layer from the HYCOM solution (units are in Nm^{-3}).

Similarly, the effect of the bottom friction boundary condition is approximated by a distributed bottom friction body force with a coefficient γ non-zero in a certain depth range ($r_{\min} < r < r_b$).

With incorporating the boundary conditions as the source terms, Eq. 18 becomes

$$\frac{2\Omega}{r}\left[\sin\theta v_\theta + \frac{\cos\theta}{r}\frac{\partial\left(r^2 v_r\right)}{\partial r}\right] + \frac{a_h}{r^2}\left(\frac{\partial^2\zeta}{\partial\theta^2} + \cot\theta\frac{\partial\zeta}{\partial\theta}\right) + a_v\frac{\partial^2\zeta}{\partial r^2} - Q^\tau - \gamma g(r)\zeta = 0. \qquad (22)$$

Here the bottom vertical profile function $g(r) = \mathrm{H}(r_{\min}) - \mathrm{H}(r_b)$ is non-zero in the interval $r_{\min} < r < r_b$ ($r_{\min} = R - H_{\max}$, $r_b = R - H_b$, $H_{\max} = 5000$, $H_b = 2500$ m) and H is the Heaviside function.

2.3.2 Scale separation

The HYCOM solution is further analyzed next, with the goal to extract most significant features which will be amenable to reduced-order modelling. The scaling of parameters is derived directly from the HYCOM simulation.

First, as illustrated in Fig. 5, the time-, vertically (layer-), and zonally averaged zonal velocity component of the HYCOM solution reveals a structure with two leading meridional wavenumbers. By defining a normalized meridional wave number, $k_\theta = \frac{K_\theta}{K_{\min}} = \frac{\lambda_{\max}}{\lambda_\theta} = \frac{R(\theta_2 - \theta_1)}{\lambda_\theta}$, where R is the Earth's mean radius, λ_θ is the corresponding wavelength in the meridional direction, $K_{\min} = \frac{2\pi}{\lambda_{\max}}$, and $\lambda_{\max} = R(\theta_2 - \theta_1)$, the two leading wavenumbers of the velocity distribution correspond to a large scale component, $k_\theta = 1$ and a small-scale component, $k_\theta = 10$. It can be remarked that the emergence of such a distinct structure with low leading wavenumbers is due the fact the Fourier transform is performed after averaging the flow in the time and zonal direction. Instantaneous snapshots of the wavenumber spectrum do not show the same leading wavenumbers. Since the instantaneous flow field is noisier than the time-averaged one, a longer time averaging of the instantaneous wavenumber spectra would be required to obtain the same spectrum as by first applying the time averaging and then the spatial Fourier transform operation.

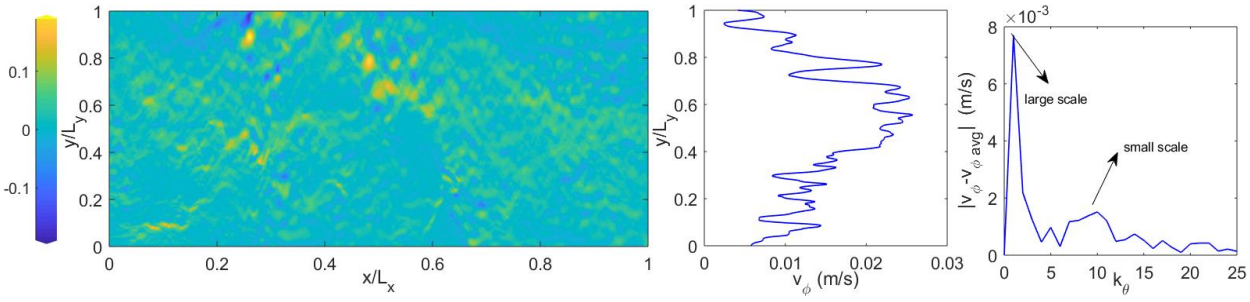

(a) (b) (c)

Fig. 5 Distributions of the zonal velocity from the HYCOM solution: (a) the time and vertically (layer-) averaged zonal velocity (ms^{-1}) within the solution domain, (b) the time-, zonally and layer-averaged zonal velocity profile, and (c) the meridional wavenumber spectrum of the time-, zonally and layer-averaged zonal velocity anomaly. The time and vertical averaging corresponds to a one-year period, using 5-day snapshots, and 41 ocean layers.

A further detailed analysis of the vorticity and its meridional gradient shows the same two length scales in the meridional wavenumber spectra. The amplitude of the vorticity spectra of the small- and the large-scale peaks are of the same order of magnitude (Fig. 6, top panel). However, the peak

in the vorticity gradient spectra corresponding to the small scale is an order of magnitude larger than that of the large scale (Fig. 6, bottom panel). This is expected since small-scale vorticity varies more rapidly with respect to the meridional coordinate and, hence, has a larger derivative ($k_\theta = 10$ vs $k_\theta = 1$ in small-scale and large-scale components, respectively). Denoting the small-scale vorticity component by $\zeta^{(l)}$ and the large-scale component by $\zeta^{(L)}$, Fig. 6 results can be summarized as

$$\begin{aligned} &\zeta^{(l)} \gg \zeta^{(L)}, \\ &\frac{\partial \zeta^{(L)}}{\partial \theta} \gg \varepsilon \frac{\partial \zeta^{(l)}}{\partial \theta}, \end{aligned} \tag{23}$$

where ε is 10^{-1} and reflects the ratio of wavenumbers (k_θ) in the two vorticity components.

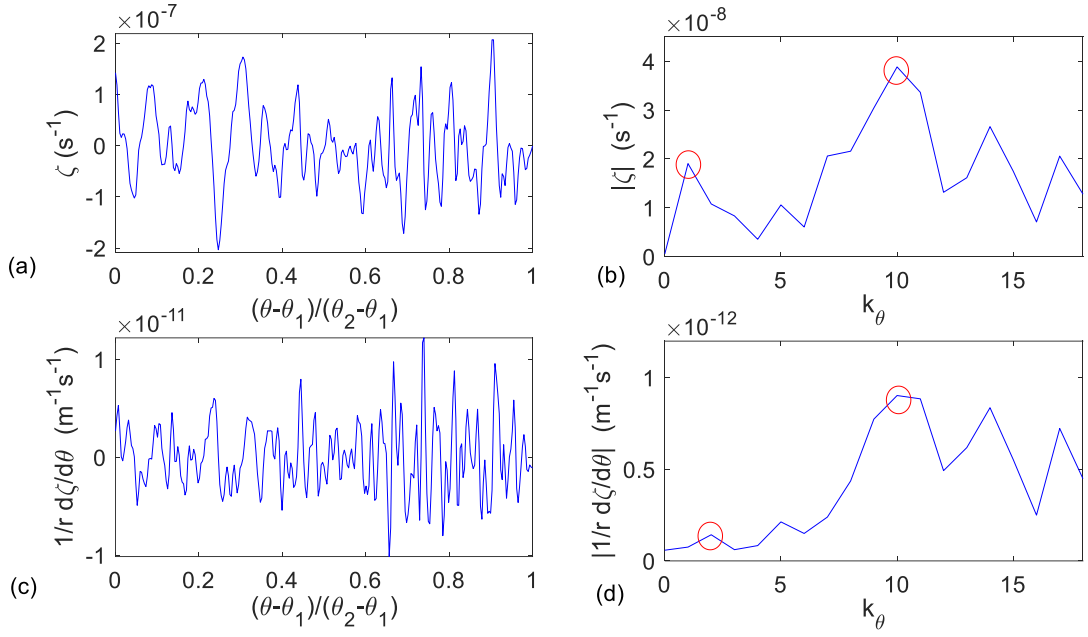

Fig. 6 Two meridional scales emerging from vorticity in the HYCOM simulations. Top: time, layer and zonally averaged vorticity versus meridional coordinate (a) and the wavenumber spectrum of the same (b). Bottom: time, layer and zonally averaged values of the vorticity meridional gradient versus meridional coordinate (c) and its wavenumber spectrum (d).

In addition, the vertical layer structure of the HYCOM solution reveals that the peak amplitude associated with the large-scale vorticity strongly depends on the layer (depth) while the peak

associated with the small-scale is nearly independent of the depth (Fig. 7). This suggests that the bottom friction is mostly affecting the large-scale component of the vorticity solution in comparison with its small-scale counterpart. The latter effect is a consequence of the linear bottom friction used in the HYCOM simulation [22]. As extracted from the numerical HYCOM solution, the difference between the values of the second-order vertical derivative in the small-scale and large-scale vorticity components is approximately one order of magnitude

$$\frac{\partial^2 \zeta^{(l)}}{\partial r^2} \approx \varepsilon \frac{\partial^2 \zeta^{(L)}}{\partial r^2}, \tag{24}$$

where ε is 10^{-1}.

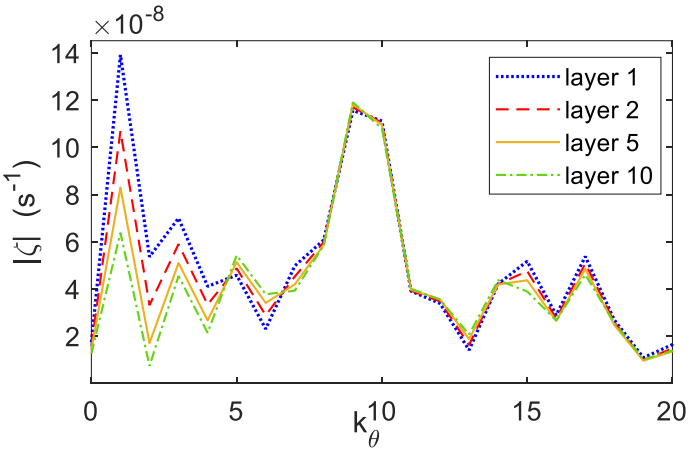

Fig. 7 Dependence of the time and zonally-averaged vorticity spectrum on the model layer.

Inspired by HYCOM simulations shown in Figs 5-7, we decompose the vorticity solution into a small-scale and a large-scale component

$$\zeta = \zeta^{(l)} + \zeta^{(L)}, \tag{25}$$

and substitute Eq. (25) in Eq. (22). Eq. (22) is then rendered dimensionless as follows

$$\frac{2\Omega H^2 V_\theta}{a_v RZ}\frac{1}{r^*}\sin\theta v_\theta^* + \frac{2\Omega H V_r}{a_v Z}\frac{\cos\theta}{r^{*2}}\frac{\partial\left(r^{*2}v_r^*\right)}{\partial z^*} + \frac{a_h}{a_v}\frac{H^2}{l^2}\frac{1}{r^{*2}}\left(\frac{\partial^2\zeta^{*(l)}}{\partial\theta^{*2}} + \frac{l}{R}\cot\theta\frac{\partial\zeta^{*(l)}}{\partial\theta^*} + \frac{\partial^2\zeta^{*(L)}}{\partial\theta^{*2}} + \frac{l}{R}\cot\theta\frac{\partial\zeta^{*(L)}}{\partial\theta^*}\right) + \left(\frac{\partial^2\zeta^{*(l)}}{\partial z^{*2}} + \frac{\partial^2\zeta^{*(L)}}{\partial z^{*2}}\right) - \frac{\tau_{\phi_{\max}} H}{a_v Z l}\frac{f^*\left(r^*\right)}{r^*}\left[\frac{1}{\sin\theta}\frac{\partial}{\partial\theta^*}\left(\sin\theta\tau_\phi^*\right)\right] - \frac{\gamma H H_b}{a_v}g^*\left(r^*\right)\zeta^{*(L)} = 0, \tag{26}$$

using the variable $z = r - r_{\min} = r - (R - H_{\max})$ ($\frac{z}{R} \ll 1$) for depth and by introducing the following dimensionless variables

$$
\begin{aligned}
&r = Rr^*,\ \mathrm{d}z = H\mathrm{d}z^*,\\
&\theta = \frac{(\theta_2 - \theta_1)}{k_\theta}\theta^*,\ r\mathrm{d}\theta = \frac{R(\theta_2 - \theta_1)}{k_\theta} r^* \mathrm{d}\theta^* = l\, r^* \mathrm{d}\theta^*,\\
&\zeta^{(l)} = Z\zeta^{*(l)},\ \zeta^{(L)} = Z\zeta^{*(L)},\\
&f(r) = \frac{H_w}{H} f^*(r^*),\ g(r) = \frac{H_b}{H} g^*(r^*),\\
&v_\theta = V_\theta v_\theta^*,\ v_r = V_r v_r^*,\ \tau_\phi = \tau_{\phi\max}\tau_\phi^*,
\end{aligned}
\tag{27}
$$

where, Z, V_θ, V_r are maximum values of vorticity, meridional velocity and radial (vertical) velocity, respectively, H is a length scale in the vertical direction and l is the meridional length scale of the zonal jets ($k_\theta = 10$). Here, we assume $a_v = 5\times10^{-3}\ \mathrm{m^2 s^{-1}}, a_h^L = 118\ \mathrm{m^2 s^{-1}}, \gamma = 10^{-7}\ \mathrm{s^{-1}}$ as provided by the HYCOM description [22]. The magnitudes of meridional velocity V_θ and vorticity $Z \sim \frac{V_\phi}{l}$ (Eq. 11) are derived from the HYCOM solution. The magnitude of zonal velocity V_ϕ is also linked to wind forcing amplitude in NAVGEM solution by $\tau_{\phi\max} \sim \frac{a_v V_\phi^{\text{top surface}}}{H_w}$ (Eq. 19) where $V_\phi^{\text{top surface}} \sim \frac{V_\phi H}{H_w}$ and we have $\frac{\partial \tau_\phi^*}{\partial \theta^*} \sim \frac{1}{k_\theta}$. In addition, the vertical velocity magnitude is related to the meridional velocity magnitude through $\frac{V_r}{H} \sim \frac{V_\theta}{R(\theta_2 - \theta_1)}$ according to the continuity equation in a periodic channel configuration (Eq. 5). It should be that $V_\theta \sim \varepsilon V_\phi$ as previously shown in Fig. 3.

Using the above definitions, the order of magnitude analysis of the coefficients in the governing vorticity equation (26) based on the maximum velocity, vorticity, and dissipation values delineates two groups of terms

$$
\begin{aligned}
&\frac{\tau_{\phi_{\max}}}{a_v Z}\frac{H}{l}\frac{1}{k_\theta} \approx \frac{\gamma H H_b}{a_v} \approx O\left(10^0\right),\\
&\frac{a_h}{a_v}\frac{H^2}{l^2} \approx \frac{2\Omega H V_r}{a_v Z} \approx \frac{2\Omega H^2 V_\theta}{a_v R Z} \approx O\left(10^{-1}\right).
\end{aligned}
\tag{28}
$$

The first group includes the dissipative term involving the second-order vorticity derivative in the vertical direction, the wind stress, and the bottom friction. The second group includes the Coriolis and meridional derivative terms.

By combining all the above arguments and following the multiscale approach of [34, 35], the governing vorticity equation (22) is decomposed into two parts, the large-scale and the small-scale vorticity equations:

$$\frac{\partial^2 \zeta^{*(L)}}{\partial z^{*2}} = \begin{cases} \dfrac{\tau_{\phi_{\max}}}{a_v}\dfrac{H}{Zl}\dfrac{1}{r^*}\left[\dfrac{1}{\sin\theta}\dfrac{\partial}{\partial\theta^*}\left(\sin\theta\tau_\phi^{\,*}\right)\right], & r_w < r < R, \\ 0, & r_b < r < r_w, \\ \dfrac{\gamma H H_b}{a_v}\zeta^{*(L)}, & r_{\min} < r < r_b, \end{cases} \tag{29}$$

$$\frac{2\Omega H^2 V_\theta}{a_v RZ}\frac{1}{r^*}\sin\theta v_\theta^{\,*} + \frac{2\Omega H V_r}{a_v Z}\frac{\cos\theta}{r^{*2}}\frac{\partial\left(r^{*2}v_r^{\,*}\right)}{\partial z^*} + \frac{a_h H^2}{a_v l^2}\frac{1}{r^{*2}}\left(\frac{\partial^2\zeta^{*(l)}}{\partial\theta^{*2}} + \frac{l}{R}\cot\theta\frac{\partial\zeta^{*(l)}}{\partial\theta^*}\right) + \frac{\partial^2\zeta^{*(l)}}{\partial z^{*2}} = 0. \tag{30}$$

Reverting the large-scale and small-scale equations back to their dimensional forms, the following equations can be obtained

$$a_v\frac{\partial^2\zeta^{(L)}}{\partial r^2} = \begin{cases} \dfrac{1}{rH_w}\left[\dfrac{1}{\sin\theta}\dfrac{\partial}{\partial\theta}\left(\sin\theta\tau_\phi\right)\right], & r_w < r < R, \quad (a) \\ 0, & r_b < r < r_w, \quad (b) \\ \gamma\zeta^{(L)}, & r_{\min} < r < r_b, \quad (c) \end{cases} \tag{31}$$

$$\frac{2\Omega}{r}\left[\sin\theta v_\theta + \frac{\cos\theta}{r}\frac{\partial\left(r^2 v_r\right)}{\partial r}\right] + \frac{a_h}{r^2}\left(\frac{\partial^2\zeta^{(l)}}{\partial\theta^2} + \cot\theta\frac{\partial\zeta^{(l)}}{\partial\theta}\right) + a_v\frac{\partial^2\zeta^{(l)}}{\partial r^2} = 0. \tag{32}$$

Equation (31) states that the vertical dissipation of the relative vorticity is balanced by the vorticity input from surface winds and bottom friction. The equation is solved by integration in the vertical direction. For integration, a factorization $\zeta^{(L)}(r,\theta) = R_L(r)\Theta_L(\theta)$ is applied where the meridional function $\Theta_L(\theta)$ is assumed to be the same as in the wind stress curl and is, thus, derived from the NAVGEM solution (see Eqs. 20-21 and Fig. 4). This substitution reduces the governing problem to an ordinary differential equation in the vertical direction, which can be integrated numerically using the boundary conditions in accordance with the NAVGEM model.

The small-scale vorticity equation (32) involves advection of planetary vorticity, vertical stretching and small-scale vorticity dissipation. From a technical point of view, the solution of (32) is more complicated than the solution of the large-scale balance. It requires solving the non-homogeneous partial differential equation

$$\frac{a_h}{r^2}\left(\frac{\partial^2\zeta^{(l)}}{\partial\theta^2}+\cot\theta\frac{\partial\zeta^{(l)}}{\partial\theta}\right)+a_v\frac{\partial^2\zeta^{(l)}}{\partial r^2}=F, \tag{33}$$

representing a traditional linear vorticity balance where the term

$$F=F_1+F_2, \tag{33a}$$

includes the advection of planetary vorticity (beta-term), $F_1=-\frac{2\Omega\sin\theta v_\theta}{r}$ and the vertical stretching term, $F_2=-\frac{2\Omega\cos\theta}{r^2}\frac{\partial\left(r^2v_r\right)}{\partial r}$.

It should be noted that the latter source term includes important non quasi-geostrophic effects, which result in additional fine-scale mixing. The effects of mixing will be balanced by viscous dissipation, as will be discussed in the numerical results section.

To eliminate the radial velocity component from the equation, the latter term can be rewritten in terms of the meridional velocity v_θ, $F_2=\frac{2\Omega\cot\theta}{r}\frac{\partial\left(\sin\theta v_\theta\right)}{\partial\theta}$, using the continuity equation (5) in a zonally averaged periodic channel.

First, to find a solution to the homogenous part of Eq. 33, we use separation of variables $\zeta^{(l)}(r,\theta)=R_l(r)\Theta_l(\theta)$ to obtain

$$\frac{a_h}{r^2}\left(R_l\Theta_l''+\cot\theta R_l\Theta_l'\right)+a_vR_l''\Theta_l=0. \tag{34}$$

After a rearrangement, (34) reduces to

$$\frac{a_h}{a_vr^2}\frac{\Theta_l''+\cot\theta\Theta_l'}{\Theta_l}=-\frac{R_l''}{R_l}=-\frac{1}{\lambda^2}. \tag{35}$$

The resulting solution components $R_l(r)$ and $\Theta_l(\theta)$ satisfy the ordinary differential equations as follows:

$$\frac{a_h}{r^2}\left(\Theta_l'' + \cot\theta\,\Theta_l'\right) + \frac{a_v}{\lambda^2}\Theta_l = 0, \tag{36}$$

$$R_l'' - \frac{1}{\lambda^2}R_l = 0, \tag{37}$$

where the constant parameter λ is computed by fitting the exponential function to the vertical distribution obtained from the small-scale vorticity component in the HYCOM simulations,

$$R_l = R_l^{\circ}\, e^{\lambda(r-R)}. \tag{38}$$

By substituting (38) into the small-scale equation (33) the latter is rearranged to an ordinary differential form,

$$\frac{a_h}{r^2}\left(\frac{\partial^2\zeta^{(l)}}{\partial\theta^2} + \cot\theta\frac{\partial\zeta^{(l)}}{\partial\theta}\right) + \frac{a_v}{\lambda^2}\zeta^{(l)} = F. \tag{39}$$

Since a_h is a non-linear function of the zonal velocity gradient, using Eq. 11, the vorticity equation (39) is rearranged in terms of the single dependent variable $v_\phi^{(l)}$ for solution,

$$\frac{a_h}{r^3}\left[\frac{\partial^3 v_\phi^{(l)}}{\partial\theta^3} + 2\cot\theta\frac{\partial^2 v_\phi^{(l)}}{\partial\theta^2} - \left(2+\cot^2\theta\right)\frac{\partial v_\phi^{(l)}}{\partial\theta} + \frac{\cos\theta}{\sin^3\theta}v_\phi^{(l)}\right] + \frac{a_v}{\lambda^2 r}\left(\frac{\partial v_\phi^{(l)}}{\partial\theta} + v_\phi^{(l)}\cot\theta\right) = F. \tag{40}$$

Once the term F is known from HYCOM data, the resulting ordinary differential equation (40) is solved numerically as an initial-value problem using the 5th order Runge-Kutta scheme.

In the solution process, the northern boundary condition corresponds to an inflection point where $\frac{\partial^2 v_\phi^{(l)}}{\partial\theta^2}|_{\theta=\theta_1} = v_\phi^{(l)}|_{\theta=\theta_1} = 0$ and the first-order derivative $\frac{\partial v_\phi^{(l)}}{\partial\theta}|_{\theta=\theta_1}$ is evaluated from the small-scale vorticity component of the HYCOM solution.

Notably, equation (40) permits harmonic-type solutions similar to the meridionally distributed alternating jets shown in Fig. 5b. Such alternating zonal jets were observed in shear driven channel flows in the previous literature [7, 8, 9].

The solutions to equations 31 and 40 are obtained by multiplying corresponding r and θ functions following separation of variables ($\zeta^{(L)}(r,\theta)=R_L(r)\Theta_L(\theta)$ and $\zeta^{(l)}(r,\theta)=R_l(r)\Theta_l(\theta)$) and finally need to be superposed to obtain the total vorticity (Eq. 25).

To summarize, guided by the scale separation observed in the spectral analysis of HYCOM solution and using scale analysis, we derived equations 31 and 40 from the vorticity equation (Eq 18) for large- and small-scale vorticity components. To complete the two-scale model, coupling of the large- and the small-scale components is achieved through the nonlinear eddy viscosity closure for $a_h{}^T$, which involves the total velocity (Eq. 14, $\bar{S}_{ij}=\bar{S}_{ij}{}^{(L)}+\bar{S}_{ij}{}^{(l)}$ and $\bar{S}_{ij}{}^{(L)}\,\square\,\bar{S}_{ij}{}^{(l)}$). Hence, the small-scale zonal jets described by (40) are coupled to the background large-scale flow through eddy viscosity.

3. Numerical Results

3.1.Comparison with HYCOM simulations

First, the semi-analytical solution for the large-scale vorticity component (31) is compared with the distribution of the first peak in the vorticity wavenumber spectrum as a function of depth extracted from HYCOM simulations. Fig. 8 shows in all three depth regions the reduced-order model is in good agreement with the HYCOM data.

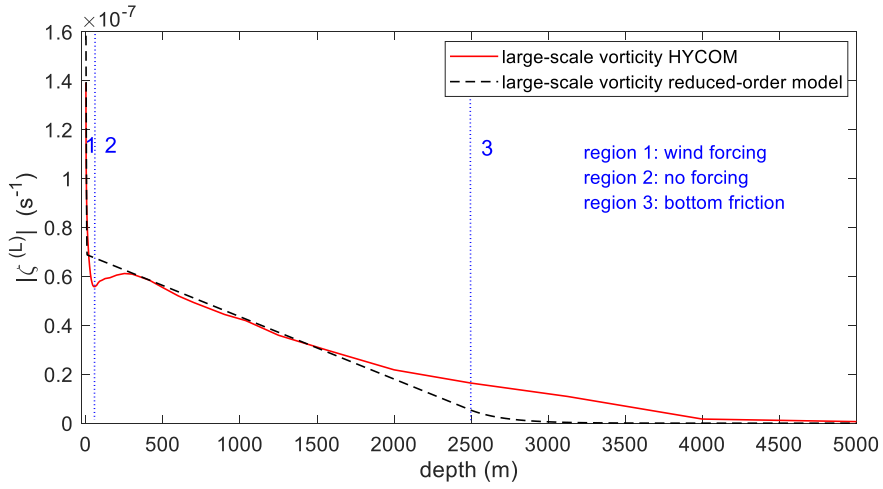

Fig. 8 The large-scale vorticity as a function of depth in the reduced-order model and HYCOM simulations.

Next, Eq.40 is solved where the source terms, $F_1 = -\frac{2\Omega \sin\theta v_\theta}{r}$ and $F_2 = \frac{2\Omega \cot\theta}{r}\frac{\partial(\sin\theta v_\theta)}{\partial\theta}$ are computed from the time and zonally averaged meridional velocity v_θ of the HYCOM solution (Fig. 3). Notably, the direct computation of $\frac{\partial v_\theta}{\partial\theta}$ in the F_2 term involves numerical differentiation of a small-amplitude quantity ($|v_\theta| \ll |v_\phi|$), which is a noisy operation due to the fine scales involved. The noise occurs due to the insufficient vertical resolution of the HYCOM solution, which was interpolated into z-level coordinates while varying locally in the zonal and meridional directions depending on the bottom topography.

To counteract the fine-scale vertical stretching term F_2 in the framework of the reduced-order model, the coefficients a_v and a_h are adjusted so that the viscous balance is explicitly preserved. Specifically, we represent the source term *F* by a random noise forcing with the variance extracted from the meridional velocity distribution in the HYCOM data and this reduces Eq.40 to a Langevin model. The latter model was originally developed to describe the Brownian motion of particles in viscous liquids, where the balance of deterministic dissipation and random fluctuation due to particle-particle collisions fully determines how the variance of the particle coordinate evolves in time [36]. In the present case, the meridional ocean coordinate is used as the homogeneous evolution variable of the Langevin equation instead of time and the small-scale vorticity is used instead of the particle coordinate. Then the values of dissipation coefficients a_v and a_h, which are required to preserve the desired meridional variance of vorticity in accordance with the HYCOM data, are evaluated following the Langevin theory (see details in the Appendix). After this, the computed dissipation coefficients a_v and a_h are substituted in Eq (40), which is integrated numerically with the Runge-Kutta method as outlined in Section 2.3.2.

Figs. 9 and 10 compare results of the two-scale model (31) and (40), using the turbulence eddy viscosity coefficient $C_s = 0.2$, with the HYCOM solution. Fig.9a shows the time-, vertically- and zonally- averaged zonal velocity profiles and Fig. 9b shows the wavenumber spectra of the velocity fluctuations for the reduced-order model and the reference HYCOM solution. The fluctuations are calculated with respect to the mean flow (i.e. the meridional average). Figs. 10 show the same comparisons as Figs. 9 but for the vorticity. Figs 11 and 12 present time- and zonally averaged

profiles and wavenumber spectra for the zonal velocity and vorticity in the top layer in comparison with the corresponding solution components of the HYCOM dataset.

It can be noted that the velocity and vorticity profiles predicted by the reduced-order model are in good agreement with the HYCOM simulations. Furthermore, the first peak, corresponding to the large-scale solution component, and the 10th peak, corresponding to the small-scale solution component (wavelength of 256 km), in the velocity and vorticity spectra of the reduced-order model are in excellent agreement with reference HYCOM data.

Good agreement for the velocity and vorticity distributions in the top layer between the model predictions and the HYCOM data also confirms that the dissipation coefficients a_h and a_v and boundary conditions in Eq.40 have been defined consistently.

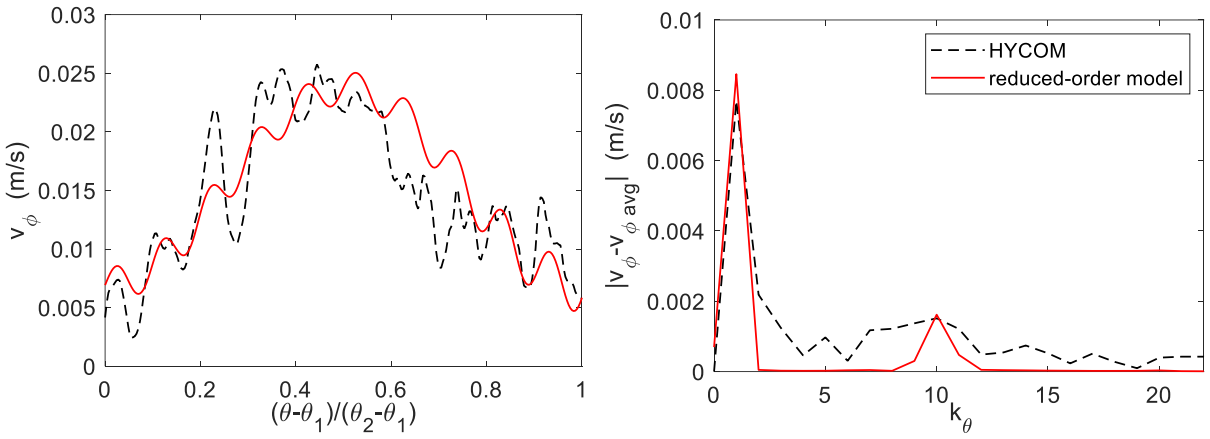

(a) (b)

Fig. 9 Comparison of the reduced-order model solutions with the HYCOM data for the time-, vertically- and zonally averaged zonal velocity (a) and the corresponding wavenumber spectrum (b).

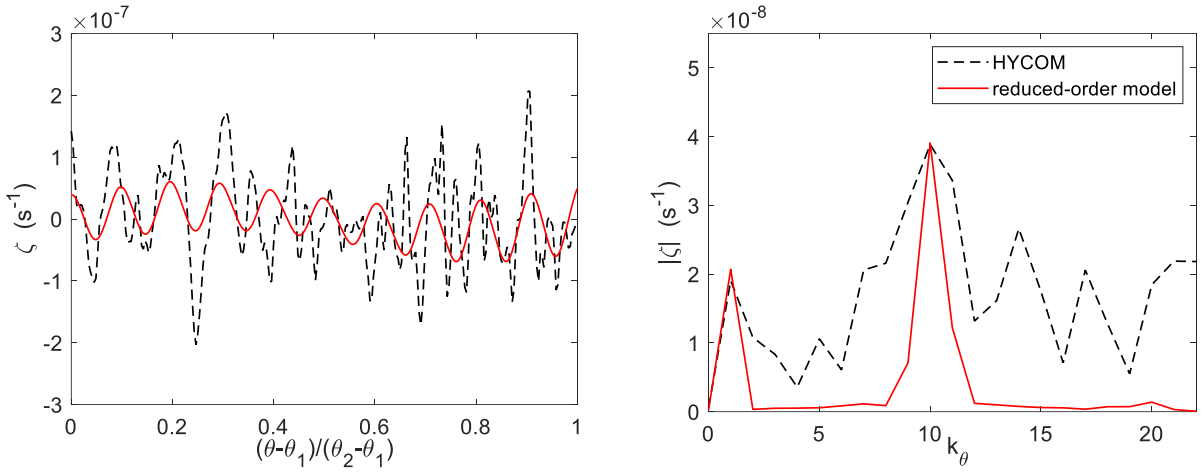

(a) (b)

Fig. 10 Comparison of the reduced-order model solutions with the HYCOM data for the time-, vertically- and zonally averaged vorticity profile (a) and the corresponding wavenumber spectrum (b).

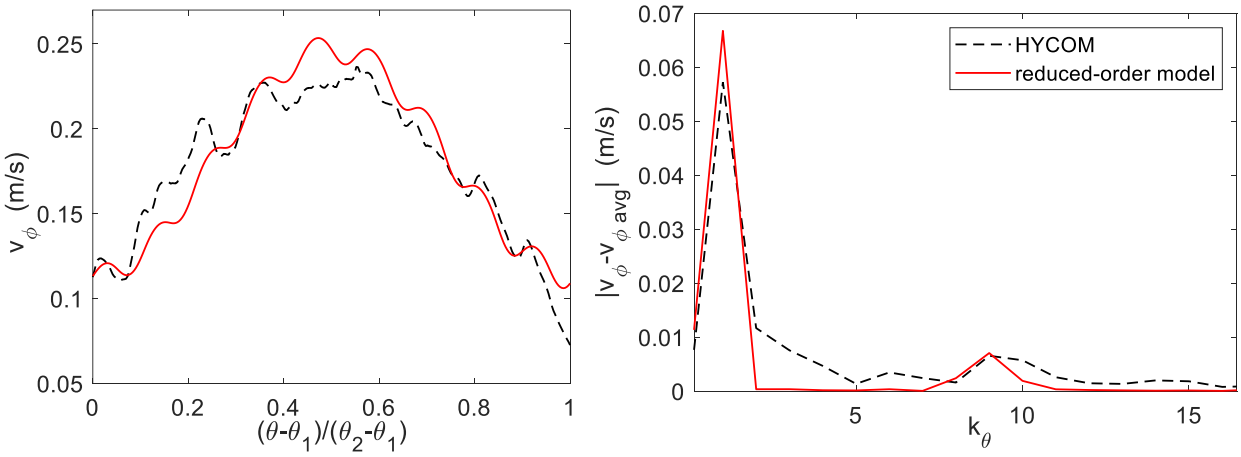

(a) (b)

Fig. 11 Comparison of the reduced-order model solutions with the HYCOM data for the time- and zonally averaged zonal velocity (a) and the corresponding wavenumber spectrum (b) in the top layer.

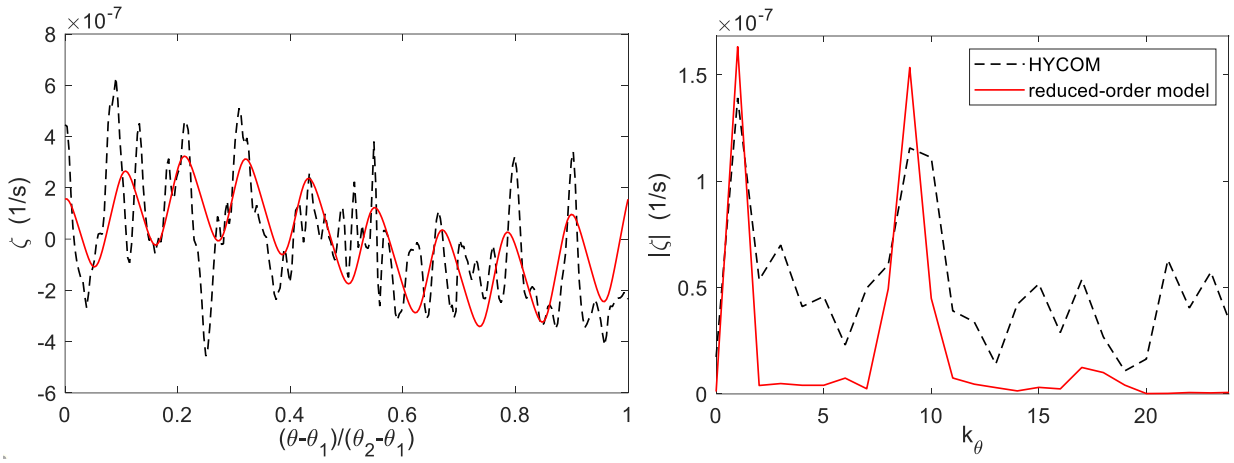

(a) (b)

Fig. 12 Comparison of the reduced-order model solutions with the HYCOM data for the time- and zonally averaged vorticity (a) and the corresponding wavenumber spectrum (b) in the top layer.

3.2. Comparison with the quasi-geostrophic model of the zonal channel

To test the robustness of the suggested reduced-order model as well as obtain further insights into the importance of non quasi-geostrophic effects such as those included in the large vertical stretching term extracted from the HYCOM simulation, the same model is also applied to reconstruct the solution of an idealized quasi-geostrophic model. In contrast to the HYCOM model, the quasi-geostrophic model considers an idealized flow domain corresponding to a shear-driven zonal re-entrant channel. As outlined in Section 2.2, the quasi-geostrophic model includes three vertical layers and a flat bottom topography and is designed to represent main features of the flow in the HYCOM simulations.

Specifically, large-scale forcing in the quasi-geostrophic model was imposed by a background shear rather than wind stress. This background flow corresponds to the large-scale zonal velocity in the reduced order-model, $v_\phi^{(L)} = \text{constant}$, and hence Eq. 31 is not required in this case. In addition, the quasi-geostrophic model simulates zonal jets (Fig. 2) that are similar to their counterparts in the more complex HYCOM model. With a suitable recalibration of parameters, the small-scale

equation in the reduced order model (Eq. 40) can describe the zonal jet structure in the quasi-geostrophic model as well as HYCOM.

To solve Eq. 40, a_h^L is directly replaced by the lateral viscosity parameter $\nu = 10\ \mathrm{m^2 s^{-1}}$ in Eq. 2 and the turbulence eddy viscosity coefficient is adjusted to $C_s = 0.75$. Similar to the HYCOM case, the eddy viscosity term couples the small-scale equation to the background constant flow. The advection of planetary vorticity F_1 and the vertical stretching term F_2 are computed from the time and zonally averaged meridional velocity v_θ and its meridional gradient as well as the constant $\beta = 1.3\times10^{-11}\mathrm{m^{-1}s^{-1}}$ in the quasi-geostrophic model. Consistent with the flat bottom topography in the quasi-geostrophic model, the zonal mean meridional velocity and the F_1 term are almost zero. The magnitude of the vertical velocity is also less than $\frac{\mathrm{Ro} V_\phi H}{L}$ (where Ro is the Rossby number) and hence the zonal-mean vertical stretching term F_2 is much smaller than in the HYCOM solution. As a result, no fine-scale Langevin adjustment of the effective viscosity parameters is applied to the viscous balance of the quasi-geostrophic effects.

Similar to the procedure used for the analysis of the HYCOM simulations, the vertical distribution parameter λ is computed by matching the solution of the quasi-geostrophic model as shown in Fig. 13 from which the effective length scale $\lambda = 400\mathrm{m}$ is obtained. In the quasi-geostrophic model, the dependence of zonal jets on parameters such as bottom friction and background velocity [9] is agglomerated in the parameter λ. Furthermore, since the vertical dissipation term does not enter the quasi-geostrophic governing equation, the corresponding coefficient is assumed to have the same value as in HYCOM, $a_v = 5\times10^{-3}\ \mathrm{m^2 s^{-1}}$. Notably, the same value of the coefficient was also reported in other primitive equation models [33].

After the recalibration of the parameters of the semi-analytical model (Eq. 40) for the quasi-geostrophic zonal channel case, it is solved numerically using Runge-Kutta method as for the HYCOM model previously. Results of the semi-analytical model for the quasi-geostrophic zonal channel are shown in Figs. 14 and 15. It can be noted that the solution of the reduced-order model captures the meridional structure of zonal jets of the quasi-geostrophic model very well. In particular, the reduced-order model accurately predicts the dominant peaks of the velocity and vorticity spectra.

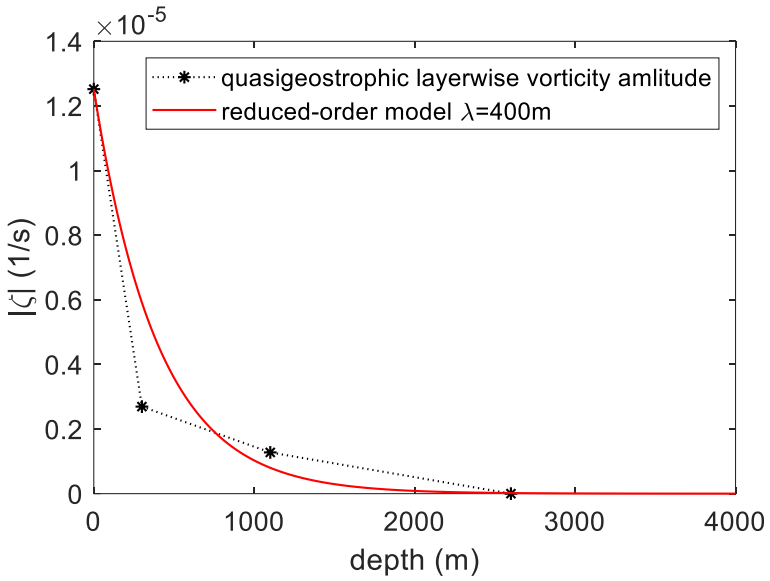

Fig. 13. Validation of the reduced-order model for the small-scale vorticity solution versus depth in comparison with the quasi-geostrophic model.

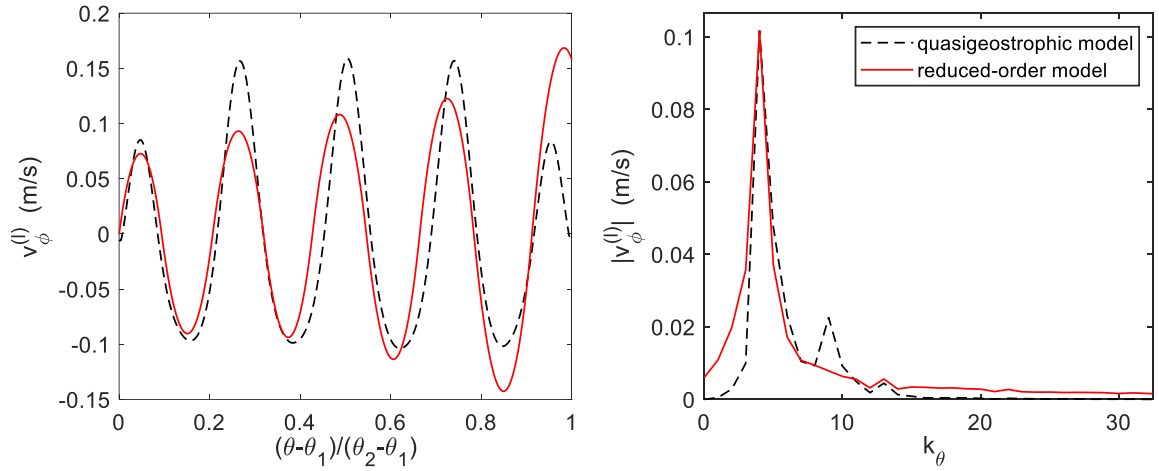

(a) (b)

Fig. 14. Comparison of the reduced-order model solutions with the quasi-geostrophic model for the time, layer and zonally-averaged zonal velocity profile (a) and the corresponding wavenumber spectrum (b).

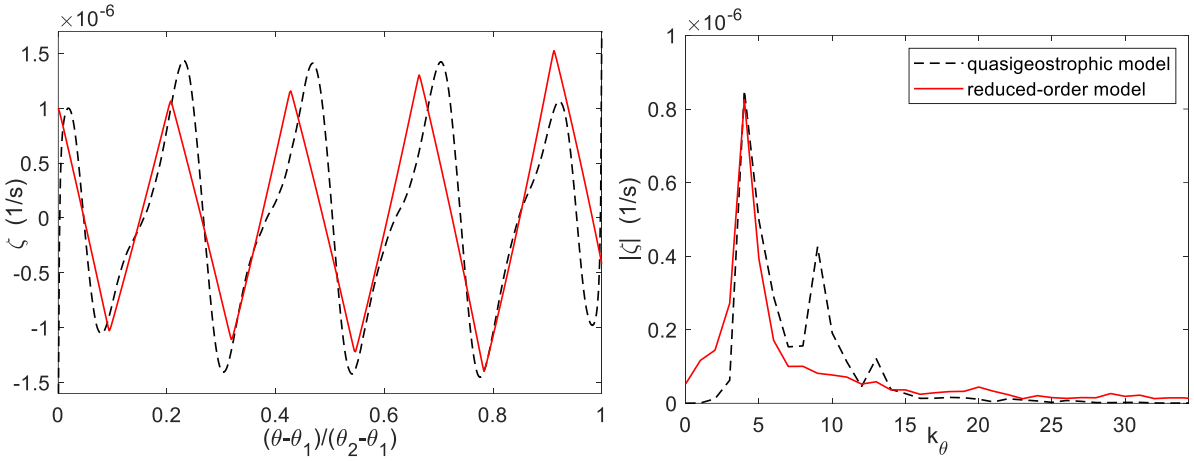

(a) (b)

Fig. 15. Comparison of the reduced-order model solutions with the quasi-geostrophic model for the time, layer and zonally-averaged vorticity profile (a) and the corresponding wavenumber spectrum (b).

4. Conclusion

Time- and zonally averaged properties of multiple zonal jets in the Southern Ocean are examined through developing a semi-analytical model that is based on the two-scale flow decomposition approach. The development of the model is informed by a high-fidelity HYCOM numerical simulation of the Southern Ocean region. The results of the semi-analytic model are further compared with an idealized quasi-geostrophic model configured for the same ocean region. The semi-analytical quasi-linear model captures the main two features of the flow: the large-scale zonal current and multiple alternating zonal jets. To implicitly represent nonlinear effects in the HYCOM model, the suggested two-scale model uses a combination of suitably calibrated Smagorinsky eddy-viscosity and Langevin dissipation model. The latter is especially important for capturing non-quasi-geostrophic effects such as those due to the vertical stretching term.

This framework allows preserving important features of the simulated flow such as the spatial distribution of zonal jets and their wavenumber spectra in a semi-analytical model ideally suitable for parametric studies. To probe the robustness of the suggested semi-analytical model and obtain

physical insights on the importance of non-quasi-geostrophic effects, the reduced-order model is further applied to a quasi-geostrophic model of the same oceanic region. Despite significant differences between assumptions and numerical approximations used in HYCOM and the quasi-geostrophic channel model, the current reduced-order model can capture pertinent features of the zonal jets and elucidate the viscous balance in each case.

In contrast to several existing dynamical models of zonal jets based on idealized linear and nonlinear dynamics [13-15, 37] the suggested semi-analytical model is derived from full solutions. It combines correlated large-scale and uncorrelated small-scale forcing to explicitly consider the viscous balance at each scale, which is required to maintain zonal jets in a statistically stationary regime. Following this approach, it is shown that, despite complexity of the underlying physics, zonal jets effectively exhibit a quasi-linear harmonic behavior, where the advection of planetary vorticity and the vertical stretching term are balanced by horizontal and vertical viscous mixing. This results in a viscous balance driven by both quasi-geostrophic effects, such as those induced by the large-scale wind forcing and non quasi geostrophic effects, due to the vertical motions and dissipation.

In future work, the suggested reduced-order model may be extended to elucidate the importance of viscous effects at different spatial scales in closed or semi-closed ocean basins, such as the Pacific Ocean where zonal jets coexist with gyre circulations.

Acknowledgements: The work of SEN was supported by InterRidge (International corporation on Ridge-crest studies) Postdoctoral Fellowship. Fundamental Research: The manuscript is not "subject" to the EAR – Fundamental Research as per EAR Part 734.8 (a) and (c).

References:

[1] Cravatte, S., Kessler, W.S., Marin, F., 2012. Intermediate zonal jets in the tropical Pacific Ocean observed by Argo floats. J. Phys. Oceanogr. 42(9), 1475-1485.

[2] Maximenko, N.A., Bang, B., Sasaki, H., 2005. Observational evidence of alternating zonal jets in the world ocean. Geophys. Res. Lett. 32(12).

554 [3] Huang, H. P., Kaplan, A., Curchitser, E.N., Maximenko, N. A., 2007. The degree of anisotropy
555 for mid-ocean currents from satellite observations and an eddy-permitting model simulation. J.
556 Geophys. Res. Oceans. 112(C9).

557 [4] Maximenko, N.A., Melnichenko, O.V., Niiler, P. P., Sasaki, H., 2008. Stationary mesoscale
558 jet-like features in the ocean. Geophys. Res. Lett. 35(8).

559 [5] Richards, K.J., Maximenko, N.A., Bryan, F. O., Sasaki, H., 2006. Zonal jets in the Pacific
560 Ocean. Geophys. Res. Lett. 33.3.

561 [6] Sinha, B., Richards, K.J., 1999. Jet structure and scaling in Southern Ocean models. J. Phys.
562 Oceanogr. 29(6), 1143-1155.

563 [7] Berloff, P., Kamenkovich, I., Pedlosky, J., 2009. A model of multiple zonal jets in the oceans:
564 Dynamical and kinematical analysis. J. Phys. Oceanogr. 39(11), 2711-2734.

565 [8] Kamenkovich, I., Berloff, P., Pedlosky, J., 2009. Role of eddy forcing in the dynamics of
566 multiple zonal jets in a model of the North Atlantic. J. Phys. Oceanogr. 39(6), 1361-1379.

567 [9] Berloff, P., Karabasov, S., Farrar, J. T., Kamenkovich, I., 2011. On latency of multiple zonal
568 jets in the oceans. J. Fluid Mech. 686, 534-567.

569 [10] Galperin, B., Nakano, H., Huang, H. P., Sukoriansky, S., 2004. The ubiquitous zonal jets in
570 the atmospheres of giant planets and Earth's oceans. Geophys. Res. Lett. 31(13).

571 [11] Condie, S.A., Rhines, P.B., 1994. A convective model for the zonal jets in the atmospheres
572 of Jupiter and Saturn. Nature, 367(6465), 711.

573 [12] Sukoriansky, S., Galperin, B., Dikovskaya, N., 2002. Universal spectrum of two-dimensional
574 turbulence on a rotating sphere and some basic features of atmospheric circulation on giant planets.
575 Phys. Rev. Lett. 89(12), 124501.

576 [13] Kaspi, Y., Flierl, G.R., 2007. Formation of jets by baroclinic instability on gas planet
577 atmospheres. J. Atmos. Sci. 64(9), 3177-3194.

578 [14] Farrell, B.F., Ioannou, P.J., 2008. Formation of jets by baroclinic turbulence. J. Atmos. Sci.
579 65(11), 3353-3375.

580 [15] Berloff, P., Kamenkovich, I., Pedlosky, J., 2009. A mechanism of formation of multiple zonal
581 jets in the oceans. J. Fluid Mech. 628, 395-425.

582 [16] Connaughton, C. P., Nadiga, B. T., Nazarenko, S. V., Quinn, B. E., 2010. Modulational
583 instability of Rossby and drift waves and generation of zonal jets. J. Fluid Mech. 654, 207-231.

584 [17] Rhines, P. B., 1975. Waves and turbulence on a beta-plane. J. Fluid Mech. 69(3), 417-443.

585 [18] Scott, R. K., Dritschel, D. G., 2012. The structure of zonal jets in geostrophic turbulence. J.
586 Fluid Mech. 711, 576-598.

587 [19] Danilov, S., Gurarie, D., 2002. Rhines scale and spectra of the β-plane turbulence with bottom
588 drag. Phys. Rev. E. 65(6), 067301.

589 [20] Nadiga, B.T., 2006. On zonal jets in oceans. Geophys. Res. Lett. 33(10).

590 [21] Huang, H.P., Robinson, W.A., 1998. Two-dimensional turbulence and persistent zonal jets in
591 a global barotropic model. J. Atmos. Sci. 55(4), 611-632.

592 [22] Wallcraft, A.J., Metzger, E.J., Carroll, S.N., 2009. Software Design Description for the
593 HYbrid Coordinate Ocean Model (HYCOM) Version 2.2.

594 [23] Smolarkiewicz, P.K., Clark, T.L., 1986. The multidimensional positive definite advection
595 transport algorithm: Further development and applications. J. Comput. Phys.67(2), 396-438.

596 [24] Smolarkiewicz, P.K., Grabowski, W.W., 1990. The multidimensional positive definite
597 advection transport algorithm: Nonoscillatory option. J. Comput. Phys. 86(2), 355-375.

598 [25] Brydon, D., Sun, S., Bleck, R., 1999. A new approximation of the equation of state for
599 seawater, suitable for numerical ocean models. J. Geophys. Res. Oceans. 104(C1), 1537-1540.

600 [26] Mellor, G.L., 1998. Users guide for a three dimensional, primitive equation, numerical ocean
601 model. Princeton, NJ: Program in Atmospheric and Oceanic Sciences, Princeton University.

602 [27] Mellor, G.L., Yamada, T., 1982. Development of a turbulence closure model for

603 geophysical fluid problems. Rev. Geophys. 20(4), 851-875.

[28] Karabasov, S.A., Goloviznin, V.M., 2009. Compact accurately boundary-adjusting high-resolution technique for fluid dynamics, J. Comput. Phys. 228(19) 7426-7451.

[29] Karabasov, S.A., Berloff, P.S., Goloviznin, V.M., 2009. CABARET in the ocean gyres. Ocean Model. 30(2-3), 155-168.

[30] Pedlosky, J., 2013. Geophysical fluid dynamics. Springer Science & Business Media.

[31] Smagorinsky, J., 1963. General circulation experiments with the primitive equations: I. the basic experiment, Mon. Weather Rev., 91(3) 99-164.

[32] Lilly, D.K., 1967. The representation of small-scale turbulence in numerical simulation experiments. IBM Form, 195-210.

[33] Dijkstra, H.A., Oksuzoglu, H., Wubs, F.W., Botta, E. F., 2001. A fully implicit model of the three-dimensional thermohaline ocean circulation J. Comput. Phys. 173(2), 685-715.

[34] Naghibi, S.E., Karabasov, S.A., Jalali, M.A., Sadati, S.H., 2019. Fast spectral solutions of the double-gyre problem in a turbulent flow regime. Appl. Math. Model. 66, 745-767.

[35] Naghibi, S.E., Jalali, M.A., Karabasov, S.A., Alam, M.R., 2017. Excitation of the Earth's Chandler wobble by a turbulent oceanic double-gyre. Geophys. J. Int. 209(1), 509-516.

[36] Van Kampen, N.G., 1992. Stochastic processes in physics and chemistry (Vol. 1). Elsevier.

[37] Rhines, P. B., 1979. Geostrophic turbulence. Ann. Rev. Fluid Mech., 11(1), 401-441.

Appendix A: A Cartesian representation of the reduced-order model in beta plane

Here, we present the reduced-order governing equations in the Cartesian coordinate system (x,y,z) attached to the local beta-plane encompassing x (west to east) and y (south to north) directions and perpendicular to the vertical axis z. The z coordinate is related to the radial coordinate in spherical coordinate system according to $z=r-r_{\min}=r-(R-H_{\max})$. The velocity vector components are given by $\mathbf{v}=(u,v,w)$ satisfying the continuity equation

$$\frac{\partial u}{\partial x}+\frac{\partial v}{\partial y}+\frac{\partial w}{\partial z}=0. \tag{A1}$$

The evolution of the vertical vorticity component, $\zeta=\frac{\partial v}{\partial x}-\frac{\partial u}{\partial y}$, is given by the z component of Eq. 4 according to

$$\frac{\partial \zeta}{\partial t}=-\frac{2\Omega}{r}\sin\theta v+2\Omega\cos\theta\frac{\partial w}{\partial z}+I^{\mathrm{conv}}(u,v)+a_h{}^L\left(\frac{\partial^2\zeta}{\partial x^2}+\frac{\partial^2\zeta}{\partial y^2}\right)+a_v\frac{\partial^2\zeta}{\partial z^2}, \tag{A2}$$

where the nonlinear term is $I^{\mathrm{conv}}(u,v)=-u\frac{\partial\zeta}{\partial x}-v\frac{\partial\zeta}{\partial y}$ and $a_h{}^L$ and a_v are the horizontal and vertical viscosity coefficients. Using the variable change $\tau=\frac{\pi}{2}-\theta$ for the latitudinal angle and linearizing the trigonometric terms around the midlatitude, Eq. A2 can be written as

$$\frac{\partial \zeta}{\partial t}=-\beta v+(f_0+\beta y)\frac{\partial w}{\partial z}-u\frac{\partial\zeta}{\partial x}-v\frac{\partial\zeta}{\partial y}+a_h{}^L\left(\frac{\partial^2\zeta}{\partial x^2}+\frac{\partial^2\zeta}{\partial y^2}\right)+a_v\frac{\partial^2\zeta}{\partial z^2}, \tag{A3}$$

where $\beta=\frac{2\Omega}{R}$, $f_0=2\Omega\sin\tau_0$ and $\tau_0=\frac{\pi-(\theta_1+\theta_2)}{2}$.

Despite similarities with the quasi-geostrophic formulation such as the low Rossby number assumption, we do not consider any restriction on vertical velocity in Eq. A3 and hence the term $\beta y\frac{\partial w}{\partial z}$ is not neglected in the equation. Eq. A3 also has a vertical dissipation term $a_v\frac{\partial^2\zeta}{\partial z^2}$ which is not typically considered in the quasigeostrophic model while it agglomerates nonlinear effects in the term $a_h{}^T$. Eq. 3 allows for smooth derivatives in the vertical direction and is neither barotropic nor stratified. Notably, our original formulation in spherical coordinates does restrict the meridional size of the domain in contrast to beta-plane approximation which is one of the key idealizations in the quasigeostrophic model.

Eq. A3 is next integrated in time and in the zonal direction x:

$$\iint\left\{\frac{\partial\zeta}{\partial t}+\beta v-(f_0+\beta y)\frac{\partial w}{\partial z}+u\frac{\partial\zeta}{\partial x}+v\frac{\partial\zeta}{\partial y}-a_h{}^L\left(\frac{\partial^2\zeta}{\partial x^2}+\frac{\partial^2\zeta}{\partial y^2}\right)-a_v\frac{\partial^2\zeta}{\partial z^2}\right\}\mathrm{d}x\,\mathrm{d}t=0, \tag{A4}$$

and the vorticity and all velocity components are decomposed into the time- and zonal-mean and fluctuation parts denoted by the overbar and primes, respectively:

$$\zeta(x,y,z,t)=\bar{\zeta}(y,z)+\zeta'(x,y,z,t), v(x,y,z,t)=\bar{v}(y,z)+v'(x,y,z,t), u(x,y,z,t)=\bar{u}(y,z)+u'(x,y,z,t). \quad \text{(A5)}$$

By definition, the mean fields satisfy

$$\begin{aligned} &\frac{\partial\bar{\zeta}}{\partial t}=\frac{\partial\bar{u}}{\partial t}=\frac{\partial\bar{v}}{\partial t}=0, \\ &\frac{\partial\bar{\zeta}}{\partial x}=\frac{\partial\bar{u}}{\partial x}=\frac{\partial\bar{v}}{\partial x}=0, \end{aligned} \quad \text{(A6)}$$

and the zonally averaged vorticity is expressed in terms of zonal velocity only $\bar{\zeta}=-\frac{\partial\bar{u}}{\partial y}$.

The difference between the time- and zonally averaged nonlinear term $\overline{I^{\mathrm{conv}}(u,v)}=-\overline{u\frac{\partial\zeta}{\partial x}}-\overline{v\frac{\partial\zeta}{\partial y}}$ and $I^{\mathrm{conv}}(\bar{u},\bar{v})$ is approximated using the turbulence eddy viscosity

$$a_h{}^T\left(\frac{\partial^2\bar{\zeta}}{\partial y^2}\right)=\overline{I^{\mathrm{conv}}(u,v)}-I^{\mathrm{conv}}(\bar{u},\bar{v}), \quad \text{(A7)}$$

where $a_h{}^T$ is the turbulent eddy viscosity coefficient computed using the classical Smagorinsky model [31] (see Eqs. 14 and 15).

Given Eqs. A6 and the small value of the zonal-mean meridional velocity in comparison with the zonal velocity in a periodic channel configuration (Fig. 3), $I^{\mathrm{conv}}(\bar{u},\bar{v})$ is neglected. Hence, the mean vorticity equation (Eq. A3) reduces to

$$-\beta v+(f_0+\beta y)\frac{\partial w}{\partial z}+\left(a_h{}^L+a_h{}^T\right)\frac{\partial^2\zeta}{\partial y^2}+a_v\frac{\partial^2\zeta}{\partial z^2}=0, \quad \text{(A8)}$$

where bars are dropped for simplicity in presentation.

With incorporating surface and bottom boundary conditions as body forces, Eq A8 becomes

$$-\beta v+(f_0+\beta y)\frac{\partial w}{\partial z}+\left(a_h{}^L+a_h{}^T\right)\frac{\partial^2\zeta}{\partial y^2}+a_v\frac{\partial^2\zeta}{\partial z^2}-Q^{\tau}-\gamma g(z)\zeta=0, \quad \text{(A9)}$$

where $Q^{\tau}=\frac{f(z)}{H_w}\frac{\partial \tau_x}{\partial y}$ is the surface wind forcing, τ_x is the wind stress in zonal direction, $f(z)=\mathrm{H}(H_{\max}-H_w)-\mathrm{H}(H_{\max})$ is the top vertical profile function in the interval $H_{\max}-H_w<z<H_{\max}$ ($H_{\max}=5000, H_w=7.5\,\mathrm{m}$), and H denotes the Heaviside step function. γ is the bottom friction coefficient and $g(z)=\mathrm{H}(0)-\mathrm{H}(H_b)$ is the bottom vertical profile function in the interval $0<z<H_b$ ($H_b=2500\,\mathrm{m}$).

Inspired by the scale separation in the spectral analysis of HYCOM solution and using an order of magnitude analysis as detailed in section 2.3.2, Eq. A9 can be decomposed into two governing equations for large-scale ($\zeta^{(L)}$) and small-scale ($\zeta^{(l)}$) vorticity components as below:

$$a_v\frac{\partial^2\zeta^{(L)}}{\partial z^2}=\begin{cases}\frac{1}{H_w}\frac{\partial\tau_x}{\partial y}, & H_{\max}-H_w<z<H_{\max}, \quad (a)\\ 0, & H_b<z<H_{\max}-H_w, \quad (b)\\ \gamma\zeta^{(L)}, & 0<z<H_b, \quad (c)\end{cases} \tag{A10}$$

$$a_h\frac{\partial^2\zeta^{(l)}}{\partial y^2}+a_v\frac{\partial^2\zeta^{(l)}}{\partial z^2}=\beta v-(f_0+\beta y)\frac{\partial w}{\partial z}=F_1+F_2, \tag{A11}$$

where $a_h=a_h{}^L+a_h{}^T$.

Appendix B: A Langevin model of the effective dissipation for the small-scale vorticity distribution

By assuming that the multiple jet structure in the θ–direction is quasi-periodic, the second-order vorticity derivative is approximated by $\frac{\partial^2\zeta^{(l)}}{\partial\theta^2}\approx -m^2\zeta^{(l)}$. With this approximation, Eq. 33 becomes

$$\frac{a_h}{r^2}\left(-m^2\zeta^{(l)}+\cot\theta\frac{\partial\zeta^{(l)}}{\partial\theta}\right)+\frac{a_v}{\lambda^2}\zeta^{(l)}=F, \tag{B1}$$

which can be expressed in terms of $\tau=\frac{\pi}{2}-\theta$ as

$$\frac{a_h}{r^2}\left(-m^2\zeta^{(l)}-\tan\tau\frac{\partial\zeta^{(l)}}{\partial\tau}\right)+\frac{a_v}{\lambda^2}\zeta^{(l)}=F. \tag{B2}$$

Equation B2 can be re-arranged to the Langevin equation form,

$$\frac{\partial \zeta^{(l)}}{\partial \tau} = -\alpha_1 \zeta^{(l)} + f, \tag{B3}$$

where $\alpha_1 = \left(m^2 - \frac{a_v r^2}{a_h \lambda^2} \right) \cot\tau > 0$ and $f = -\frac{r^2 \cot\tau}{a_h} F$, wherein F is given by (33a).

According to the Langevin model, the first term, $-\alpha_1 \zeta^{(l)}$ corresponds to the energy dissipation and the second term, f corresponds to the stochastic forcing, which generates energy to be balanced by the dissipation.

In accordance with HYCOM data, the random forcing has approximately zero mean, $\langle f(\tau) \rangle = 0$ and is uncorrelated, i.e. $\langle f(\tau) f(\tau') \rangle = \Gamma \delta(\tau - \tau')$ with Γ being the strength of the Langevin force term.

Following [36], the solution of Eq. (B3) is

$$\zeta^{(l)}(\tau) = \zeta_0{}^{(l)} e^{-\alpha_1 \tau} + e^{-\alpha_1 \tau} \int_0^{\tau} e^{\alpha_1 \tau'} f(\tau') d\tau', \tag{B4}$$

where $\zeta^{(l)}(0) = \zeta_0{}^{(l)}$ corresponds to vorticity at $\tau = \tau_1 = \frac{\pi}{2} - \theta_1$ and the variance of $\zeta^{(l)}(\tau)$ is given by

$$\left\langle \zeta^{(l)}(\tau) \right\rangle^2 = \left(\zeta_0{}^{(l)^2} - \frac{\Gamma}{2\alpha_1} \right) e^{-2\alpha_1 \tau} + \frac{\Gamma}{2\alpha_1}. \tag{B5}$$

To ensure that $\left\langle \zeta^{(l)}(\tau) \right\rangle^2$ is bounded, the condition $\Gamma = 2\alpha_1 \zeta_0{}^{(l)^2}$ must be satisfied. This means that, in equilibrium, the strength of the fluctuating force is balanced by the dissipation according to

$$\zeta_0{}^{(l)^2} = \frac{\mathrm{var}(F)}{2\left(\frac{a_h}{r^2}\right)^2 \left(m^2 - \frac{a_v r^2}{a_h \lambda^2} \right) \cot\theta}. \tag{B6}$$

Notably, to obtain the meridional vorticity variance in accordance with the HYCOM dataset, the denominator in (B6) needs to be adjusted accordingly. It follows that the ratio of dissipation parameters, $\frac{a_v}{a_h}$ can be kept the same as in the HYCOM description [22] while simultaneously

703 scaling a_v and a_h to attain the same vorticity variance as the HYCOM data. The scaling of a_h

704 applies to both linear and nonlinear parts ${a_h}^L$ and ${a_h}^T$.

705 The dissipation coefficient value a_h which is needed to balance the effect of the forcing $F = F_1 + F_2$

706 in the solution of the small-scale vorticity equation (33) is then given by

707 $$a_h = \sqrt{\frac{\mathrm{var}(F)}{2\frac{{\zeta_0^{(l)}}^2}{r^4}\left(m^2 - \frac{a_v r^2}{a_h \lambda^2}\right)\cot\theta}}. \qquad \text{(B7)}$$